PHOTONICS Research

Passively mode-locked Er-doped fiber laser based on SnS$_2$ nanosheets as a saturable absorber

Kangdi Niu,[1] Ruyi Sun,[1] Qingyun Chen,[1] Baoyuan Man,[1] and Huanian Zhang[1,2,*]

[1]Shandong Provincial Key Laboratory of Optics and Photonic Devices, School of Physics and Electronics, Shandong Normal University, Jinan 250014, China
[2]Institute of Data Science and Technology, Shandong Normal University, Jinan 250014, China
*Corresponding author: huanian_zhang@163.com

In this paper, tin disulfide (SnS$_2$), a two-dimensional (2D) n-type direct bandgap layered metal dichalcogenide with a gap value of 2.24 eV, was employed as a saturable absorber. Its appearance and nonlinear saturable absorption characteristics were also investigated experimentally. SnS$_2$-PVA (polyvinyl alcohol) film was successfully prepared and employed as a mode-locker for achieving a mode-locked Er-doped fiber laser with a pulse width of 623 fs at a pulse repetition rate of 29.33 MHz. The results prove that SnS$_2$ nanosheets will have wide potential ultrafast photonic applications due to their suitable bandgap value and excellent nonlinear saturable absorption characteristics.   © 2018 Chinese Laser Press

1. INTRODUCTION

Recently, two-dimensional (2D) materials, including graphene [1–5], carbon nanotubes [6–9], topological insulators [10–14], transition metal dichalcogenides [15–20], and black phosphorus [21–23], have been widely employed as saturable absorbers (SAs) for demonstrating passively Q-switched or mode-locked fiber lasers. Especially, various TMDs (MoS$_2$ [15,16], WS$_2$ [17,18], MoSe$_2$ [19,20], WSe$_2$ [19,20]) have been extensively used as a mode-locker for achieving mode-locked Yb, Er, and Tm-doped fiber lasers due to their advantages of unusual electronic and structural properties, wide absorption range, and ultrafast recovery time. Recently, IV–VI group TMDs, including SnSe$_2$ and ReS$_2$, have held certain attention in the fields of ultrafast optics due to their suitable layer-independent bandgap value and anisotropic crystal structure. Thereinto, by employing the SnSe$_2$-coated mirror as a saturable absorber, passively Q-switched lasing within a crystalline waveguide platform at ~1 μm was reported by Cheng et al. [24]. In 2017, Mao et al. reported an ReS$_2$-polyvinyl alcohol (PVA) film based passively Q-switched and mode-locked erbium-doped fiber laser [25]. Obviously, studies on the application of IV–VI group TMDs in achieving ultrafast pulse lasers are still in their infancy. Therefore, it is of great significance and urgency to expand the ultrafast nonlinear optical applications of IV–VI group TMDs.

Tin disulfide (SnS$_2$) was an n-type direct bandgap semiconductor with a value of 2.24 eV; it has a CdI$_2$ crystal structure, and the sandwich structure consists of two layers of close-packed sulfur anions and one-layer tin cations [26–29].

Previously, its low-cost, environmentally friendly, Earth-abundant characteristics made it better to fulfill industrial and scientific requirements in the fields of solar cells, photocatalysts, lithium-ion batteries, and so on. However, to our knowledge, the nonlinear optical absorption properties of SnS$_2$ have been rarely reported. Due to its suitable bandgap value of 2.24 eV, which corresponds to the visible optical region, SnS$_2$ is expected to have the same saturable absorption characteristics as the reported TMDs (MoS$_2$, WS$_2$, MoSe$_2$, WSe$_2$).

In this paper, SnS$_2$-PVA film was successfully prepared and employed as a mode-locker in obtaining an Er-doped mode-locked laser. Its appearance and nonlinear saturable absorption characteristics were investigated; the saturation intensity and modulation depth were about 125 MW/cm^2 and 4.6%, respectively. Based on the SnS$_2$-PVA film as SA, a mode-locked Er-doped fiber laser operating at the central wavelength of 1562.01 nm with a 3 dB bandwidth of 6.09 nm was demonstrated; the pulse width was 623 fs with a pulse repetition rate of 29.33 MHz. The experimental results prove that, in comparison with the reported TMDs, SnS$_2$ has analogous saturable absorption characteristics and equal excellent performance in the field of ultrafast optics.

2. PREPARATION AND CHARACTERIZATION OF MATERIALS

Figure 1 shows the preparation process of the film-type SnS$_2$-PVA SA. First, an SnS$_2$ dispersion solution was prepared
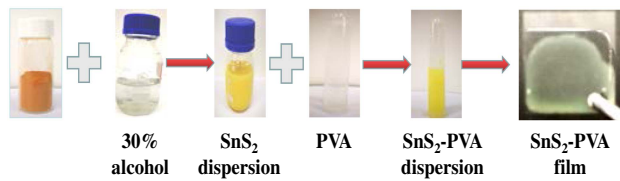
Fig. 1. Preparation process of the SnS₂-PVA film-type SAs.

by adding 1 g SnS_2 nanosheets into 100 mL alcohol (30%). After that, the mixture was placed in the ultrasonic cleaner for 12 h and then centrifuged at a rate of 2000 rpm for 30 min to remove the deposit. Then, the SnS_2 dispersion and 4 wt. % PVA solution were mixed at the volume ratio of 1 : 2; the mixture was placed in the ultrasonic cleaner for 4 h to obtain the SnS_2-PVA dispersion solution. Afterward, 200 μL SnS_2-PVA dispersion solution was spin-coated on a sapphire substrate. The coated substrate was placed into an oven for 48 h at 30 °C. Then, a thin SnS_2-PVA film was obtained. Finally, a 1 mm × 1 mm thin film was stripped off and put on the end face of the photonic crystal (PC) fiber head for making SAs.

The surface topography of the SnS_2 nanosheet was analyzed by a scanning electron microscope (SEM). Figure 2(a) shows the SEM image under a resolution of 60 μm; as is shown, the SnS_2 nanosheet has an obvious layered structure. Figure 2(b) shows the energy dispersion X-ray (EDX) spectroscopy of the SnS_2 nanosheet. The peaks associated with sulfur and tin are clearly observed. Additionally, the surface distribution of elements is shown in the Fig. 2(b) inset.

For testing the layered structure properties of the SnS_2 dispersion, the transmission electron microscope (TEM) image of the SnS_2 nanosheets dispersion solution has also been recorded by a JEM-2100 microscope with an optical resolution of 500 nm; as is shown in Fig. 3(a), the SnS_2 nanosheets exhibits an obvious layered structure. Additionally, Fig. 3(b) shows the selected-area electron diffraction of the SnS_2. The results, shown in Fig. 3, indicate that the SnS_2 nanosheets prepared in our work have a layered structure with high crystallinity.

The crystal structure of the SnS_2 nanosheet was characterized by X-ray diffraction (XRD). As shown in Fig. 4(a), the XRD pattern exhibits high diffraction peaks, especially for the (001) plane and does not show any diffraction peaks except for SnS_2, which indicates that SnS_2 nanosheets with a well-layered structure and high crystallinity were successfully prepared. The Raman spectrum of the layered SnS_2 is shown

Fig. 3. (a) TEM image of the SnS₂ nanosheets. (b) Selected-area electron diffraction.
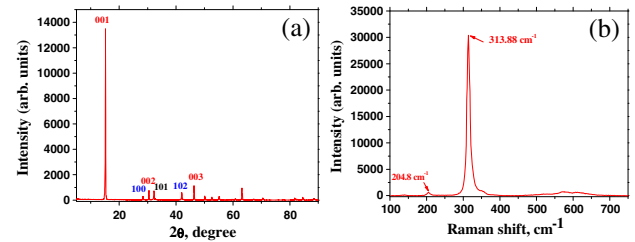
Fig. 4. (a) X-ray diffraction of the SnS₂ nanosheets. (b) Raman spectrum of the SnS₂ nanosheets.

in Fig. 4(b); apparently, two Raman shift peaks, corresponding to the A and E symmetry intralayer mode, at 313 and 205 cm^{-1}, were characterized, which is in agreement with the previously reported results [29].

The nonlinear optical properties of the prepared SnS_2-PVA film were investigated by an open-aperture Z-scan technique. The experimental setup of the Z-scan testing platform is shown in Fig. 5(a). The SnS_2 sample is irradiated by a femtosecond pulse (central wavelength: 800 nm; repetition rate: 1 Hz; pulse duration: 8 fs). An optical attenuator was used for the power controlling. A beam splitter was used to separate the incident laser power at the ratio of 50 : 50. The SnS_2-PVA film was perpendicular to the beam axis and shifted along the z axis via a linear electric platform. A lens with a focal length of 150 cm was used for generating a waist radius of 70 μm. A double-channel power meter was used for detecting the output power of different path.

Experimental and fitting results of the open-aperture Z-scan measurements are shown in Fig. 5(b). It is obvious that the open-aperture curves of normalized transmittance exhibit symmetric peak patterns around the focal point ($z = 0$), indicating the nonlinear saturable absorption of the SnS_2-PVA film.
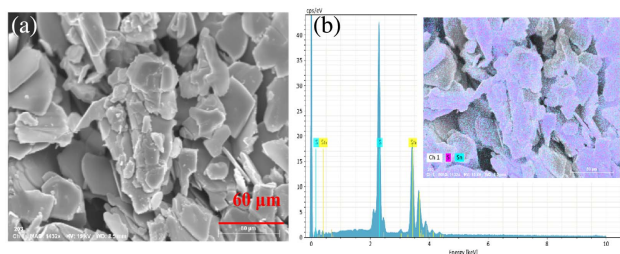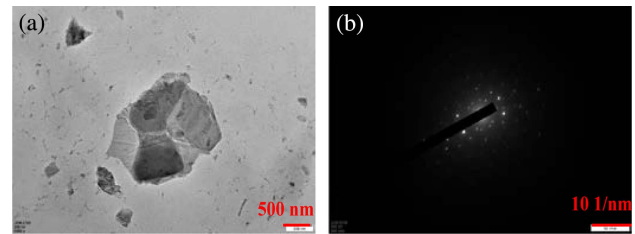

Fig. 2. (a) SEM image of the SnS₂ nanosheet. (b) EDX spectroscopy of the SnS₂ nanosheet. Inset of (b): surface distribution of elements.
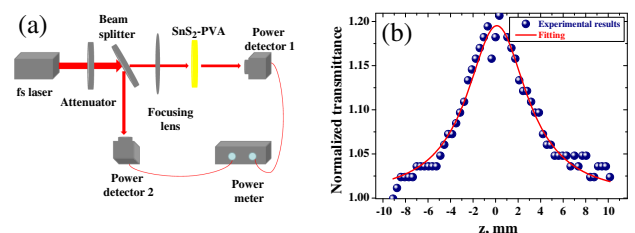

Fig. 5. (a) Experimental setup of the Z-scan testing platform. (b) Open-aperture Z-scan curves of the SnS₂-PVA film.

Additionally, the open-aperture Z-scan curves in Fig. 5(b) were fitted by using the following equation [30]:

$$T(z) = \left[1 - \frac{\alpha_0 L I_s}{I_s + I_0/(1 + z^2/z_0^2)}\right] / (1 - \alpha_0 L), \quad \textbf{(1)}$$

$$T(z) = 1 - \frac{\beta I_0 L_{\text{eff}}}{2\sqrt{2}(1 + z^2/z_0^2)}, \quad \textbf{(2)}$$

$$L_{\text{eff}} = (1 - e^{-\alpha_0 L})/\alpha_0, \quad \textbf{(3)}$$

where z is the sample position relative to the focus position, z_0 is the diffraction length of the beam, $\alpha_0 L$ is the modulation depth, $T(z)$ is the normalized transmittance at z, I_0 is peak on-axis intensity at focus, and I_s is the saturable intensity. The modulation depth of the SnS$_2$-PVA can be obtained according to the linear optical transmittance, which is shown in Fig. 6(a). The values of linear absorption coefficient α and nonlinear absorption coefficient β were 54 cm^{-1} and 9.9×10^{-10} m/W, respectively.

The transmittance of the SnS$_2$-PVA film and the substrate versus optical wavelength was investigated with a UV/Vis/NIR spectrophotometer (Hitachi U-4100) and are shown in Fig. 6(a). It is obvious that the transmission increases with the wavelength. Finally, the transmission of the SnS$_2$-PVA film at the wavelength of 1562 nm was about 86.4%. Additionally, based on a power-dependent transmission technique and a homemade nonlinear polarization rotation mode-locked Er-doped fiber laser with 560 fs pulses at 1560.3 nm and a repetition rate of 33.6 MHz, the nonlinear optical properties of the SnS$_2$-PVA film was investigated. As is shown in Fig. 6(b), the transmittance increases by 4.6% when the SnS$_2$-PVA film saturated at I_{peak} of 125 MW/cm^2, indicating that the saturation intensity and modulation depth were about 125 MW/cm^2 and 4.6%, respectively.

3. EXPERIMENTAL DETAILS

The experimental setup of the SnS$_2$-PVA based Er-doped fiber laser is shown in Fig. 7. A 980 nm laser diode (LD) with a maximum output power of 680 mW was used as the pump source. The pump energy was delivered into the cavity via a 980/1550 wave division multiplexer (WDM). A piece of 65 cm long Er-doped fiber (nlight, Er-110) with a dispersion parameter of ~ -46 ps/(km·nm) was employed as the laser gain medium. A 10:90 optical coupler (OC) was used to output
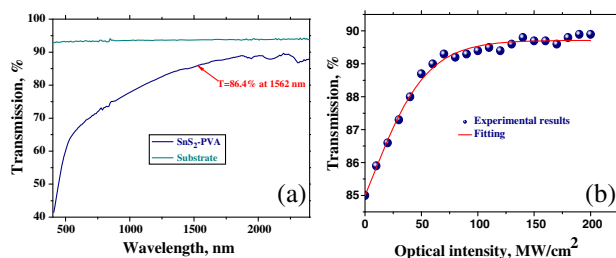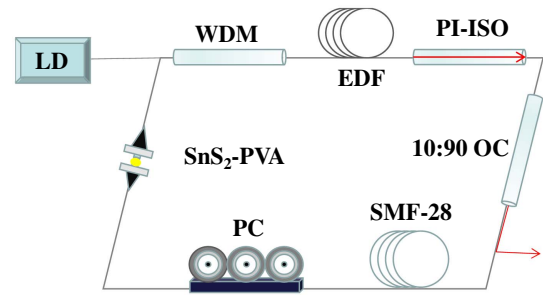

Fig. 7. Experimental setup of the mode-locked fiber laser.

the laser. A polarization-independent isolator (PI-ISO) and a polarization controller (PC) were used for unidirectional operation and adjusting the polarization state in the cavity, respectively. A 3 m long single-mode fiber (SMF) with dispersion parameter of ~ 17 ps/(km·nm) was added into the cavity for dispersion management. The total length of the cavity was about 7.0 m; thus, the net dispersion of the Er-doped fiber laser was calculated to be -0.1 ps^2.

4. EXPERIMENTAL RESULTS

In the experiment, when the pump power was higher than 125 mW, by carefully adjusting the PCs in the cavity, stable pulse trains can be recorded. The emission spectrum of the SnS$_2$-based Er-doped fiber laser, which was recorded by an optical spectrum analyzer (AQ-6317) with a resolution of 0.02 nm, is shown in Fig. 8(a). As is shown, typical soliton-like pulse shapes with characteristic Kelly sideband peaks were obtained. The central wavelength and 3 dB spectrum bandwidth were 1562.01 and 6.09 nm, respectively. The autocorrelation trace of the mode-locked operation is shown in Fig. 8(b); the measured pulse trace was well-fitted with a sech^2 profile, and their full width at half-maximum (FWHM) was 623 fs; thus, the time-bandwidth product (TBP) is about 0.466, which is a little higher than the theoretical limit value (0.315), indicating that the optical pulse is slightly chirped. Additionally, it is obvious that the operating photon energy value of our work was 0.79 eV, which was much lower than the bandgap of SnS$_2$ (2.24 eV). That is to say, the absorption was not due to the direct bandgap. Therefore, sub-bandgap absorption was responsible for the passively mode-locked operation. Actually, sub-bandgap absorption phenomena have been widely reported before [31–33]. As is known, in a perfect crystal, there is no sub-bandgap absorption. However, in a finite system, the sub-bandgap absorption at low photon energies also could be realized, which are attributed to energy levels within the
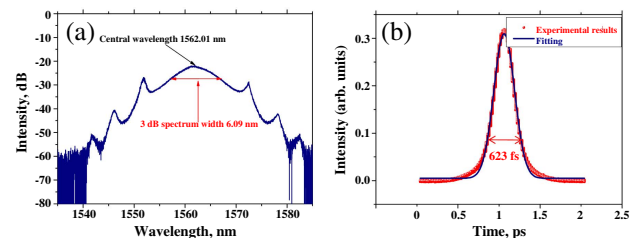

Fig. 6. (a) Linear transmission of the SnS$_2$-PVA film versus wavelength. (b) Nonlinear absorption property of the SnS$_2$-PVA film.

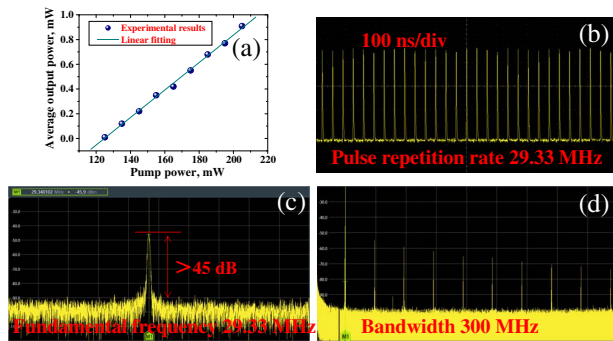**Fig. 8.** (a) Emission spectrum. (b) Autocorrelation trace.

Fig. 9. (a) Relationships between the average output power and pump power. (b) Pulse train of the mode-locked operation. (c) Radio frequency (RF) spectrum of the mode-locked laser located at 29.33 MHz. (d) RF spectrum with a bandwidth of 300 MHz.

bandgap arising from the edge-state. In our opinion, sub-bandgap absorption observed in our work was also attributed to the edge-state absorption of the SnS_2.

The relationships between the average output powers and pump powers are shown in Fig. 9(a); it is obvious that the output power and the pump power have a linear correlation. The maximum average output power was 1.2 mW under a pump power of 205 mW, corresponding to an optical conversion efficiency of 0.59%. Figure 9(b) depicts a typical pulse train of the mode-locked laser, the pulse repetition rate was 29.33 MHz, which matches well with the cavity length of 7.0 m. Additionally, stability is one of the most important parameters that restricts the practical application of the mode-locked laser. For testing the stability of the SnS_2-PVA based mode-locked laser, the radio frequency spectrum was recorded by a spectrum analyzer (R&S FPC1000); Fig. 9(c) depicts the radio frequency spectrum located at the fundamental repetition rate of 29.33 MHz with a bandwidth of 3 MHz and a resolution of 20 kHz, the signal-to-noise ratio is >45 dB. In addition, the radio frequency spectrum within a wide bandwidth of 300 MHz is shown in Fig. 9(d). All the results exhibit that mode-locked pulses with high stability were obtained in our work.

For testing the long-time stability of the fiber laser, the output spectra were recorded continuously at a 2 h interval over 10 h, as shown in Fig. 10(a). Figure 10(b) shows the central wavelength and the 3 dB spectrum bandwidth of the recorded spectra depicted in Fig. 10(a); the central wavelength was fixed within a range of less than 0.2 nm. Meanwhile, variety of the
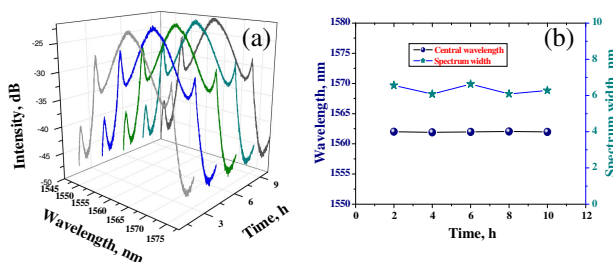

Fig. 10. (a) Emission spectra at different times. (b) Central wavelengths and spectrum widths at different times.

3 dB spectrum bandwidth was less than 0.2 nm. Clearly, this laser shows relatively good long-term stability.

5. CONCLUSION

In conclusion, SnS_2-PVA film was successfully prepared and employed as a saturable absorber within an Er-doped fiber laser for generating passively mode-locked operation. Passive mode-locking operation with an average output power of 1.2 mW and a pulse width of 623 fs under a repetition rate of 29.33 MHz was obtained. Our result exhibited that SnS_2 with a suitable bandgap value and excellent nonlinear saturable absorption characteristics will have extensively wide ultrafast photonics and optoelectronic applications.

REFERENCES

1. H. Zhang, D. Tang, R. J. Knize, L. Zhao, Q. Bao, and K. P. Loh, "Graphene mode locked, wavelength-tunable, dissipative soliton fiber laser," Appl. Phys. Lett. **96**, 111112 (2010).
2. D. Popa, Z. Sun, F. Torrisi, T. Hasan, F. Wang, and A. C. Ferrari, "Sub 200 fs pulse generation from a graphene mode-locked fiber laser," Appl. Phys. Lett. **97**, 203106 (2010).
3. Z. Sun, T. Hasan, F. Torrisi, D. Popa, G. Privitera, F. Wang, F. Bonaccorso, D. M. Basko, and A. C. Ferrari, "Graphene mode-locked ultrafast laser," ACS Nano **4**, 803–810 (2010).
4. Z. Sun, D. Popa, T. Hasan, F. Torrisi, F. Wang, E. J. R. Kelleher, J. C. Travers, and A. C. Ferrari, "A stable, wideband tunable, near transform-limited, graphene-mode-locked, ultrafast laser," Nano Res. **3**, 653–660 (2010).
5. F. Bonaccorso, Z. Sun, T. Hasan, and A. C. Ferrari, "Graphene photonics and optoelectronics," Nat. Photonics **4**, 611–622 (2010).
6. M. A. Solodyankin, E. D. Obraztsova, A. S. Lobach, A. I. Chernov, A. V. Tausenev, V. I. Konov, and E. M. Dianov, "Mode-locked 1.93 μm thulium fiber laser with a carbon nanotube absorber," Opt. Lett. **33**, 1336–1338 (2008).
7. F. Wang, A. G. Rozhin, V. Scardaci, Z. Sun, F. Hennrich, I. H. White, W. I. Milne, and A. C. Ferrari, "Wideband-tuneable, nanotube mode-locked, fibre laser," Nat. Nanotechnol. **3**, 738–742 (2008).
8. X. Zhao, Z. Zheng, L. Liu, Y. Liu, Y. Jiang, X. Yang, and J. Zhu, "Switchable, dual-wavelength passively mode-locked ultrafast fiber laser based on a single-wall carbon nanotube modelocker and intracavity loss tuning," Opt. Express **19**, 1168–1173 (2011).
9. N. Nishizawa, Y. Seno, K. Sumimura, Y. Sakakibara, E. Itoga, H. Kataura, and K. Itoh, "All-polarization-maintaining Er-doped ultrashort-pulse fiber laser using carbon nanotube saturable absorber," Opt. Express **16**, 9429–9435 (2008).
10. Z. C. Luo, M. Liu, H. Liu, X. W. Zheng, A. P. Luo, C. J. Zhao, H. Zhang, S. C. Wen, and W. C. Xu, "2 GHz passively harmonic mode-locked fiber laser by a microfiber-based topological insulator saturable absorber," Opt. Lett. **38**, 5212–5215 (2013).
11. H. Liu, X. W. Zheng, M. Liu, N. Zhao, A. P. Luo, Z. C. Luo, C. J. Zhao, and S. C. Wen, "Femtosecond pulse generation from a topological insulator mode-locked fiber laser," Opt. Express **22**, 6868–6873 (2014).
12. C. J. Zhao, Y. H. Zou, Y. Chen, Z. T. Wang, S. B. Lu, H. Zhang, S. C. Wen, and D. Y. Tang, "Wavelength-tunable picosecond soliton fiber laser with topological insulator: Bi_2Se_3 as a mode locker," Opt. Express **20**, 27888–27895 (2012).
13. Y. H. Lin, C. Y. Yang, S. F. Lin, W. H. Tseng, Q. Bao, C. I. Wu, and G. R. Lin, "Soliton compression of the erbium-doped fiber laser weakly

started mode-locking by nanoscale p-type Bi_2Te_3 topological insulator particles," Laser Phys. Lett. **11**, 055107 (2014).

14. J. Sotor, G. Sobon, W. Macherzynski, and K. M. Abramski, "Harmonically mode-locked Er-doped fiber laser based on a Sb_2Te_3 topological insulator saturable absorber," Laser Phys. Lett. **11**, 055102 (2014).

15. H. Xia, H. P. Li, C. Y. Lan, C. Li, X. X. Zhang, S. J. Zhang, and Y. Liu, "Ultrafast erbium-doped fiber laser mode-locked by a CVD-grown molybdenum disulfide (MoS_2) saturable absorber," Opt. Express **22**, 17341–17348 (2014).

16. J. Du, Q. K. Wang, G. B. Jiang, C. W. Xu, C. J. Zhao, Y. J. Xiang, Y. Chen, S. C. Wen, and H. Zhang, "Ytterbium-doped fiber laser passively mode locked by few-layer molybdenum disulfide (MoS_2) saturable absorber functioned with evanescent field interaction," Sci. Rep. **4**, 6346 (2014).

17. D. Mao, Y. D. Wang, C. J. Ma, L. Han, B. Q. Jiang, X. T. Gan, S. J. Hua, W. D. Zhang, T. Mei, and J. L. Zhao, "WS_2 mode-locked ultrafast fiber laser," Sci. Rep. **5**, 7965 (2015).

18. P. G. Yan, A. J. Liu, Y. S. Chen, J. Z. Wang, S. C. Ruan, H. Chen, and J. F. Ding, "Passively mode-locked fiber laser by a cell-type WS_2 nanosheets saturable absorber," Sci. Rep. **5**, 12587 (2015).

19. B. H. Chen, X. Y. Zhang, K. Wu, H. Wang, J. Wang, and J. P. Chen, "Q-switched fiber laser based on transition metal dichalcogenides MoS_2, $MoSe_2$, WS_2, and WSe_2," Opt. Express **23**, 26723–26737 (2015).

20. D. Mao, X. Y. She, B. B. Du, W. D. Zhang, K. Song, X. Q. Cui, B. Q. Jiang, T. Peng, and J. L. Zhao, "Erbium-doped fiber laser passively mode locked with few-layer $WSe_2/MoSe_2$ nanosheets," Sci. Rep. **6**, 23583 (2016).

21. J. Sotor, G. Sobon, M. Kowalczyk, W. Macherzynski, P. Paletko, and K. M. Abramski, "Ultrafast thulium-doped fiber laser mode locked with black phosphorus," Opt. Lett. **40**, 3885–3888 (2015).

22. Z. C. Luo, M. Liu, Z. N. Guo, X. F. Jiang, A. P. Luo, C. J. Zhao, X. F. Yu, W. C. Xu, and H. Zhang, "Microfiber-based few-layer black phosphorus saturable absorber for ultra-fast fiber laser," Opt. Express **23**, 20030–20039 (2015).

23. Y. Chen, G. B. Jiang, S. Q. Chen, Z. N. Guo, X. F. Yu, C. J. Zhao, H. Zhang, Q. L. Bao, S. C. When, D. Y. Tang, and D. Y. Fan, "Mechanically exfoliated black phosphorus as a new saturable absorber for both Q-switching and mode-locking laser operation," Opt. Express **23**, 12823–12833 (2015).

24. C. Cheng, Z. Q. Li, Z. Q. Li, N. N. Dong, J. Wang, and F. Chen, "Tin diselenide as a new saturable absorber for generation of laser pulses at 1 μm," Opt. Express **25**, 6132–6140 (2017).

25. D. Mao, X. Q. Cui, X. T. Gan, M. K. Li, W. D. Zhang, H. Lu, and J. L. Zhao, "Passively Q-switched and mode-locked fiber laser based on a ReS_2 saturable absorber," IEEE J. Sel. Top. Quantum Electron. **24**, 1100406 (2018).

26. J. Seo, J. T. Jang, S. W. Park, C. J. Kim, B. W. Park, and J. W. Cheon, "Two-dimensional SnS_2 nanoplates with extraordinary high discharge capacity for lithium ion batteries," Adv. Mater. **5**, 5226–5230 (2008).

27. B. Luo, Y. Fang, B. Wang, J. Zhou, H. Song, and L. Zhi, "Two dimensional graphene-SnS_2 hybrids with superior rate capability for lithium ion storage," Energy Environ. Sci. **5**, 5226–5230 (2012).

28. J. T. Kai, K. X. Wang, Y. Z. Su, X. F. Qian, and J. S. Chen, "High stability and superior rate capability of three-dimensional hierarchical SnS_2 microspheres as anode material in lithium ion batteries," J. Power Sources **196**, 3650–3654 (2011).

29. A. J. Smith, P. E. Meek, and W. Y. Liang, "Raman scattering studies of SnS_2 and $SnSe_2$," J. Phys. C **10**, 1321–1323 (1977).

30. J. Guo, T. Y. Ning, Y. S. Han, Y. Q. Sheng, C. H. Li, X. F. Zhao, Z. Y. Lu, B. Y. Man, Y. Jiao, and S. Z. Jiang, "Preparation, characterization, and nonlinear optical properties of hybridized graphene @ gold nanorods nanocomposites," Appl. Surf. Sci. **433**, 45–50 (2018).

31. B. Guo, Q. L. Yu, Y. Yao, and P. F. Wang, "Direct generation of dip-type sidebands from WS_2 mode-locked fiber laser," Opt. Mater. Express **6**, 2475–2486 (2016).

32. R. I. Woodward, E. J. R. Kelleher, R. C. T. Howe, G. Hu, F. Torrisi, T. Hasan, and J. R. Taylor, "Tunable Q-switched fiber laser based on saturable edge-state absorption in few-layer molybdenum disulfide (MoS_2)," Opt. Express **22**, 31113–31122 (2014).

33. S. X. Wang, H. H. Yu, H. J. Zhang, A. Z. Wang, M. W. Zhao, Y. X. Chen, L. M. Mei, and J. Y. Wang, "Broadband few-layer MoS_2 saturable absorbers," Adv. Mater. **26**, 3538–3544 (2014).